analytical chemistry

Perspective

pubs.acs.org/ac

Democratization of Nanoscale Imaging and Sensing Tools Using Photonics

Euan McLeod,[†,‡,∥] Qingshan Wei,[†,‡,∥] and Aydogan Ozcan*[,†,‡,§]

[†]Department of Electrical Engineering, University of California Los Angeles (UCLA), Los Angeles, California 90095, United States
[‡]Department of Bioengineering, University of California Los Angeles (UCLA), Los Angeles, California 90095, United States
[§]California NanoSystems Institute (CNSI), University of California Los Angeles (UCLA), Los Angeles, California 90095, United States

ABSTRACT: Providing means for researchers and citizen scientists in the developing world to perform advanced measurements with nanoscale precision can help to accelerate the rate of discovery and invention as well as improve higher education and the training of the next generation of scientists and engineers worldwide. Here, we review some of the recent progress toward making optical nanoscale measurement tools more cost-effective, field-portable, and accessible to a significantly larger group of researchers and educators. We divide our review into two main sections: label-based nanoscale imaging and sensing tools, which primarily involve fluorescent approaches, and label-free nanoscale measurement tools, which include light scattering sensors, interferometric methods, photonic crystal sensors, and plasmonic sensors. For each of these areas, we have primarily focused on approaches that have either demonstrated operation outside of a traditional laboratory setting, including for example integration with mobile phones, or exhibited the potential for such operation in the near future.

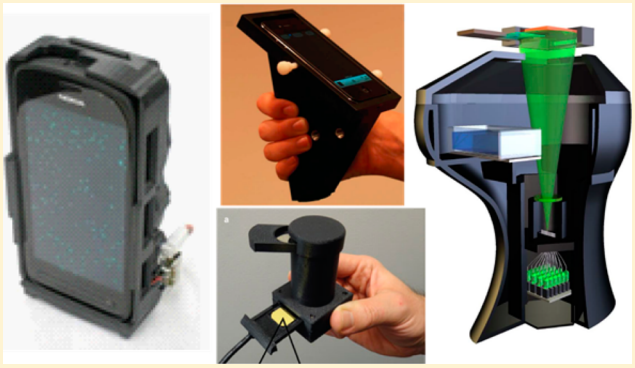

The democratization of science and technology refers to the increased involvement in these fields for those who would not normally have the opportunity or inclination due to their socioeconomic status, local environment, upbringing, or background.[1] This involvement can take the form of enhanced understanding of, appreciation of, benefit from, and contribution to science and technology. The impact of this increased participation is expected to include significantly improved education and training and an accelerated rate of discovery and invention in various fields. The development of cost-effective, field-portable, and easy-to-use, yet advanced, scientific tools can help to engender all of these impacts. Education can be strengthened through earlier and more universal exposure of students to such tools or instruments, allowing students to actively perform advanced experiments instead of just reading about them. As another potential broad impact, personal healthcare can be improved via consumer-level health monitoring and diagnostics technologies and especially by new tools that are not prohibitively expensive for use in the developing world.[2,3] Furthermore, the acceleration of scientific discovery and invention can occur both through the direct involvement of laypeople in crowd-sourced research (e.g., SETI at home,[4] bird population counting,[5,6] protein folding,[7,8] and malaria diagnostics[9−12]) or simply as a consequence of the general population being more willing to allocate public funds to research after having gained a better understanding of what scientific research is, how it is done, and why it is important. Accelerated discovery and innovation will also be a long-term consequence of the increased democratization of scientific instrumentation and toolsets, where placing the entire world on an equal educational footing will expand the number of scientists, engineers, and researchers at the forefronts of their fields. A common feature of all of these expected impacts is increased self-reliance. However, while the increased confidence from being able to make one's own scientific experiments and direct observations is laudable, the role of the expert must not be eliminated. Especially in medicine, while personal monitoring, sensing, and diagnostic tools can help to provide early warnings and more frequent biomedical testing to individuals, it should not be used as a complete substitute for professional medical evaluation and care.

One opportune area for increased democratization is that of *nanoscience* and *nanotechnology* tools, which in general have been rather costly and bulky, limiting their use to well-resourced institutions. For many laypeople, nanoscience and nanotechnology can elicit awe or trepidation, partially due to media hype about the partially unknown effects of nanomaterials in the body as well as the environment. The development and wide-scale use of tools that make measurements at the nanoscale can help to better inform and educate

Received: April 14, 2015
Accepted: June 12, 2015
Published: June 12, 2015

DOI: 10.1021/acs.analchem.5b01381
Anal. Chem. 2015, 87, 6434−6445

people about nanocience and nanotechnology. Such tools will also make it possible for untrained individuals to conduct experiments in the field or even at their homes that would have previously required advanced laboratory equipment and/or infrastructure. They can also help to further expand crowd-sourced research from what has previously been primarily an online computer-based endeavor to an in-person active experimental endeavor as people conduct some experiments and research in their own buildings and/or neighborhoods.

Here, we review some of the recent progress on translating conventional laboratory-based optical nanoscale measurement techniques into tools that can help to democratize scientific measurements by virtue of their compact, cost-effective, and easy-to-use designs. The conventional laboratory-based nanoscale measurement tools that are beginning to be translated in such ways include sensing and imaging tools that allow people to determine the sizes, concentrations, and/or compositions of nanoparticles in a given sample of interest. Some of the gold standard techniques for nanoscale measurement tools include electron microscopy and atomic force microscopy. These approaches have excellent resolving power; however, they rely on expensive and bulky equipment in addition to a well-established infrastructure and can be relatively slow with low throughput. Other types of nanoscale measurement approaches include mechanical means such as oscillating microscopic cantilevers[13] as well as electrical means such as conductivity measurements across a nanopore that permits the flow of, e.g., nanoparticles.[14] These mechanical and electrical approaches can also be implemented in compact and cost-effective forms;[15,16] however, an extended discussion of them is beyond the scope of this review, which is focused on photonics-enabled tools.

By sacrificing some resolving power for reduced cost and increased throughput, it is possible to use optical measurement tools to gain much of the same types of information (nanomaterial size, concentration, composition, etc.) as provided by electron microscopy. Optical methods are also much easier to implement on portable devices compared to electron microscopy approaches. While several cost-effective microscopy approaches have been recently developed that are capable of making *microscale* measurements, including, e.g., imagers that are integrated with mobile phones[1] or are folded out of paper,[17] in this manuscript, we will focus on the optical designs that enable nanoscale measurements and sensing.[18] Examples of conventional microscopy-based optical nanoscale measurement tools include interferometry,[19] which is capable of measuring displacements as small as $\sim 10^{-18}$ m,[20] and super-resolution microscopy such as photoactivated localization microscopy,[21] stochastic optical reconstruction microscopy,[22] or stimulated emission depletion microscopy.[23] Examples of sensing-based optical nanoscale measurement tools include dynamic light scattering,[24] nanoparticle tracking analysis,[25] laser scattering,[26,27] surface plasmon resonance biosensors,[28] optical microcavity sensors,[29] and fiber-optic or waveguide-based sensors,[30,31] among others. While many of these techniques are bound to laboratory settings due to their dependence on expensive and bulky equipment, some can be implemented in "democratization-friendly" platforms, which we review below along with "democratic" implementations of other optical measurement schemes. We divide these democratic approaches into two categories: (i) label-based approaches that use fluorescent tags to provide specificity and increased signal from nanoscale objects and (ii) label-free approaches.

Many of the approaches that we focus on below are based around *mobile phones* and in particular smartphones. Mobile phones are one of the most readily available technology platforms that can help democratize science and technology tools globally and provide the foundation for advanced nanoscale measurements. They are undergoing a Moore's-law-like growth in their capabilities while simultaneously taking advantage of the benefits of mass production and economies of scale.[1,32] For example, since the introduction of the first camera phone in around 2000,[33] the pixel count of the image sensors embedded in mobile phones has, on average, doubled every two years by following Moore's law and reached >40 megapixels up to date.[33] In the meantime, the pixel size of the mobile phone image sensor has decreased down to ~1.1 μm,[34] providing higher and higher spatial resolution even under modest magnification factors. In addition to these, the number of mobile phone subscriptions has increased to ~7 billion,[35] where 78% of these mobile phones are being used in developing countries.[35] Although much of the developing world has not yet adopted smartphones, cell phone use is ubiquitous, and as the early adopters of new technology frequently upgrade their smartphones, more and more of these used smartphones will be available, forming an expanding market for second-hand smartphones, which might further accelerate the penetration of smartphones into resource-limited settings.[1]

DEMOCRATIZATION OF LABEL-BASED NANOSCALE MEASUREMENT TOOLS

Mobile Phone-Based Wide-Field Fluorescence Imaging. Fluorescence imaging is one of the predominant label-based methods for nanoscale measurements and characterization such as nanoparticle sizing in biological media,[36] virus imaging,[37] and many others.[38−41] Fluorescence microscopy is especially attractive due to its specificity and contrast. However, conventional fluorescence microscopes are bulky and expensive and therefore not widely available for use in the field or in remote areas. Recently, mobile phone-based microscopy platforms are emerging to provide alternatives to conventional benchtop microscopes; translation of mobile phone devices into hand-held microscopy platforms relies on the creation of lightweight, compact, and mechanically robust imaging attachments that can be added onto the existing camera module of the mobile phone. These imaging attachments include optical components such as light-emitting-diodes (LEDs), lasers, lenses, and thin-film filters, all tailored depending on the application of interest. Disposable glass slides or microfluidic chips can be inserted into this opto-mechanical attachment, and in contrast to conventional imaging tools that require a desktop computer for image processing and/or visualization, the mobile phone imaging platform is able to rapidly analyze and display the captured images on a standalone and compact device, which is desired for point-of-care and field applications.

Fluorescence-based imaging modalities have been adopted on mobile phones by different optical configurations, such as Köhler illumination,[42] waveguide coupling,[43−45] orthogonal illumination,[46] or epifluorescence detection.[47] However, the detection sensitivity of the earlier mobile phone microscopy devices has been limited to microscale specimens, such as single bacilli,[42] cells,[44,48] or microspheres.[43,44] Detection of nanoscale objects with mobile phone-based imaging tools has remained a significant challenge due to the limited signal-to-noise ratio (SNR) of these previous optical designs.

DOI: 10.1021/acs.analchem.5b01381
Anal. Chem. 2015, 87, 6434−6445

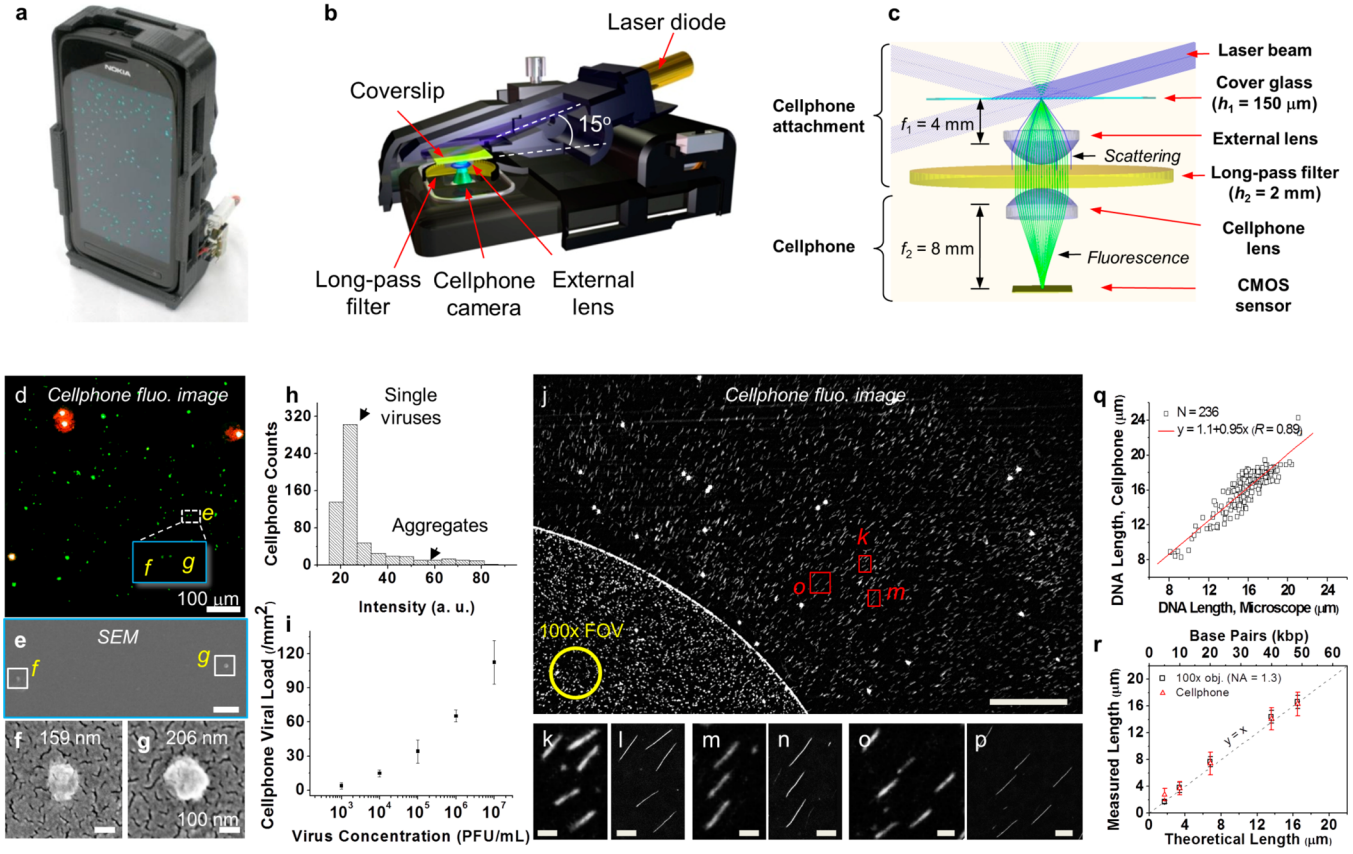

Figure 1. Mobile phone-based fluorescence microscopy. (a) Photograph of hand-held mobile imaging device. (b) Schematic illustration of high-angle illumination (~75°). (c) Optical ray tracing simulation of the mobile phone imaging device. (d) Cell phone fluorescence image of single CMV. (e–g) SEM comparison images confirm the detection of single virus particles on the mobile phone. (h) Virus particle intensity distribution measured from the cell phone image. (i) Cell phone-based viral load measurement. (j) Large field of view (~2 mm^2) cell phone fluorescence image of single λ DNA molecules that are linearly stretched. (k, m, o) Zoomed-in cell phone images. (l, n, p) Corresponding images obtained by a conventional benchtop microscope equipped with a 100× objective (NA = 1.3). (q) DNA length measured by the cell phone device vs conventional fluorescence microscope. (r) Sizing of 5 different length DNA fragments with the mobile phone device, showing a length measurement accuracy of <1 kbp for DNA strands that are longer than 10 kbp. Panels a–i are reproduced from Wei, Q.; Qi, H.; Luo, W.; Tseng, D.; Ki, S. J.; Wan, Z.; Göröcs, Z.; Bentolila, L. A.; Wu, T.-T.; Sun, R.; Ozcan, A. *ACS Nano* **2013**, *7*, 9147–9155 (ref 49). Copyright 2013 American Chemical Society. Panels j–r are reproduced from Wei, Q.; Luo, W.; Chiang, S.; Kappel, T.; Mejia, C.; Tseng, D.; Chan, R. Y. L.; Yan, E.; Qi, H.; Shabbir, F.; Ozkan, H.; Feng, S.; Ozcan, A. *ACS Nano* **2014**, *8*, 12725–12733 (ref 50). Copyright 2014 American Chemical Society.

We have recently demonstrated a new mobile phone-based fluorescence microscope design with substantially improved imaging sensitivity through suppressing background noise created by excitation leakage.[49] In this optical design, the specimen is illuminated by an oblique excitation beam delivered at an angle (e.g., 75°) that is much larger than the light collection angle of the imaging attachment of the mobile phone device (Figure 1a–c).[49] Therefore, blocking of the excitation leakage relies on the prevention of the direct excitation beam from entering the low numerical aperture (NA) imaging system. This lightweight (~186 g) opto-mechanical attachment includes an external lens (also taken from a mobile phone camera), a mini focusing stage, and a sample chamber, in addition to a laser diode and thin-film interference filter (Figure 1a,b). Using this cost-effective and hand-held fluorescence microscope, single 100 nm fluorescent nanoparticles were imaged on the mobile phone, and their sizes were independently verified by scanning electron microscopy (SEM) of the same samples.[49]

This simple, low-cost, and field-portable fluorescence microscopy platform installed on a mobile phone can also be used to detect various nonfluorescent biological objects or molecules via fluorescent labeling. In this context, we demonstrated the detection and counting of individual human cytomegalovirus (CMV) by using this handheld mobile phone fluorescence microscope after specific fluorescence labeling of the sample.[49] CMV can cause a fatal infection to immunocompromised patients such as HIV+ patients and newborn babies. Purified CMVs were labeled with primary glycoprotein B antibodies followed by Alexa 488-conjugated secondary antibodies and imaged by our mobile phone imaging device, achieving single-virus sensitivity as independently confirmed by SEM imaging of the same sample (Figure 1d–g).[49] Mobile phone-based virus density measurement has also been demonstrated by counting the number of CMVs captured on the coverslips from various concentrations of virus solutions ranging from 10^3 to 10^7 plaque forming units per mL (PFU/mL) (see Figure 1h,i). As desired, the virus density measured by the mobile phone microscope shows a strong correlation with the virus concentration of the initial solution stock.

With a similar mobile phone-based fluorescent imaging design, we have also demonstrated the imaging and sizing of single DNA molecules that are fluorescently labeled.[50] As a proof of concept, λ bacteriophage DNA (48 kilobase pairs, kbp)

DOI: 10.1021/acs.analchem.5b01381
Anal. Chem. 2015, 87, 6434–6445

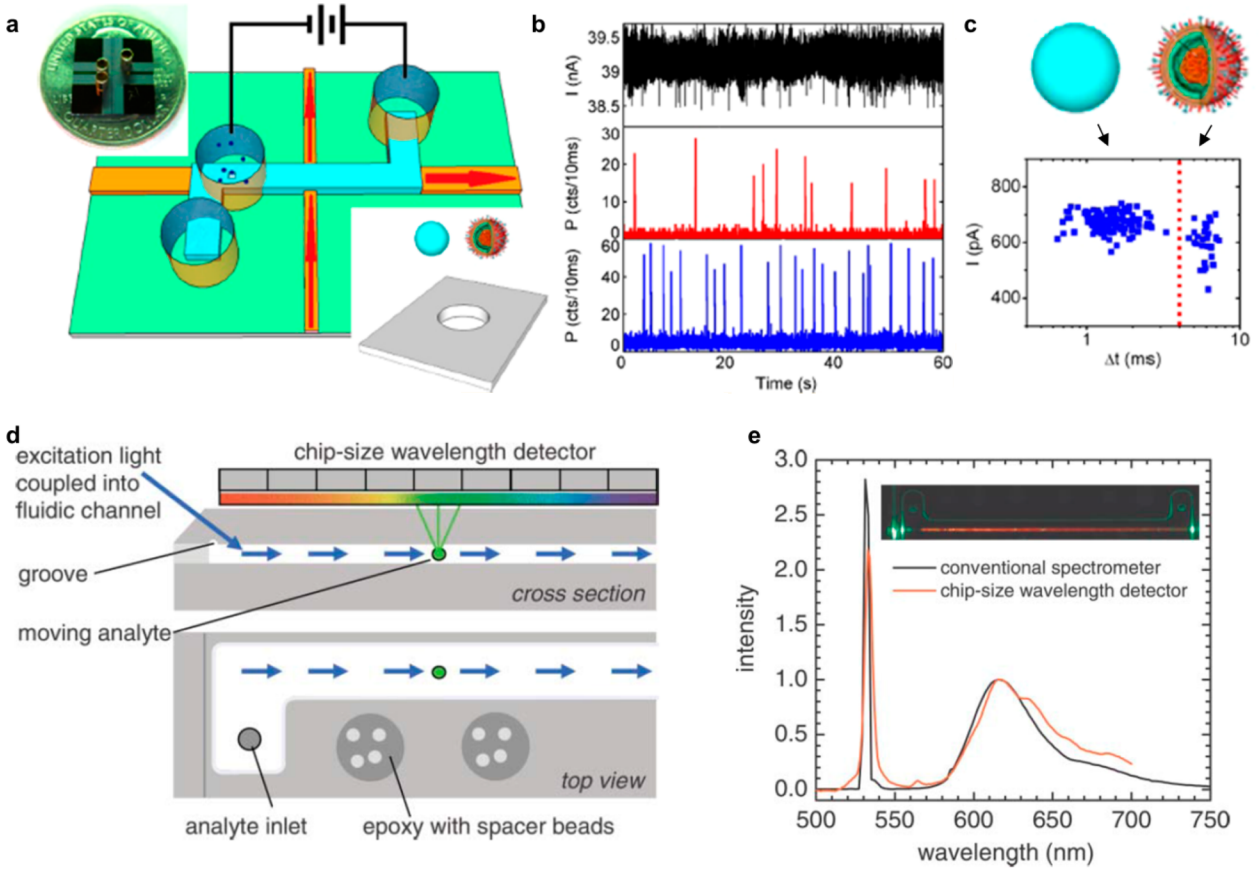

Figure 2. On-chip fluorescence-based nanoparticle sizing and characterization methods. (a) Dual-mode electrical and optical single-nanoparticle sensing platform. (b) Electrical (top) and optical fluorescence signals from viruses (center; red fluorescence) and nanobeads (bottom; blue). (c) Classification of H1N1 viruses against 100 nm fluorescent beads with the optofluidic device. (d) Microfluidic spectrometer. (e) Fluorescence spectra of Alexa633 recorded with conventional (black) and on-chip (red) spectrometer. Panels a–c are reproduced from Liu, S.; Zhao, Y.; Parks, J. W.; Deamer, D. W.; Hawkins, A. R.; Schmidt, H. *Nano Lett.* **2014**, *14*, 4816–4820 (ref 59). Copyright 2014 American Chemical Society. Panels d and e are reprinted by permission of The Royal Society of Chemistry from Schmidt, O.; Bassler, M.; Kiesel, P.; Knollenberg, C.; Johnson, N. *Lab Chip* **2007**, *7*, 626–629 (ref 60). Copyright 2007 the Royal Society of Chemistry.

was stained with an intercalating dye (YOYO-1) and linearly stretched on a planar glass coverslip by using a simple droplet compression method. Figure 1j shows a large field-of-view (FOV) cell phone fluorescence image of stretched λ DNA molecules over ~2 mm^2 area, which is about 2 orders of magnitude larger than the FOV of a conventional fluorescence microscope equipped with a 100× objective (NA 1.3).[50] The zoomed-in regions of interest (ROI) suggest that the contrast of the mobile phone fluorescence image of single DNA molecules is comparable to that of conventional fluorescence microscopy (Figure 1k–p). The FOV advantage of the mobile phone fluorescence device allows us to measure the length of thousands of single DNA molecules in a single frame.

The length measurement of each linearly stretched DNA strand is based on a custom-developed algorithm, which estimates the length of the DNA molecules by fitting each DNA segment in the cell phone image with the point spread function (PSF) of the mobile phone device. A Windows-based mobile phone application has also been created to transfer the captured fluorescence images to a remote server, which can complete the length quantification in seconds and transmit the results back to the mobile phone. Using this cost-effective mobile microscopy platform, we demonstrated our DNA length sizing accuracy to be <~0.96 kbp by imaging various lengths of DNA fragments including 10, 20, 40 (T7 DNA) and 48 kbp (λ DNA); see Figure 1q,r.[50] Such measurement capability and the accuracy of our mobile phone-based fluorescent imaging device can potentially enable us to map structural variations in DNA, including, e.g., detection of copy-number variations (CNVs) or single nucleotide polymorphisms (SNPs) at the point-of-care or even in field settings.

One of the promising directions for facilitating point-of-care applications of label-based approaches is to further simplify sample preparation and labeling steps for low infrastructure settings. The majority of current labeling approaches rely on antibody targeting or other specific biochemical recognition mechanisms whose labeling efficiency is typically diffusion rate limited. In this regard, many lab-on-a-chip techniques have recently been developed to accelerate this process in a reduced volume or by enhancing mixing with controlled microfluidics. Indeed, various sample preparation protocols have been demonstrated on a chip such as cell lysis,[51] DNA extraction,[52] and amplification.[53] Meanwhile, novel cost-effective surface functionalization methods have been emerging such as aptamer-based ligands[54,55] to replace antibody binding. All of these make label-based approaches very promising for point-of-care applications in poor resource settings.

Fluorescence-Based Nanoparticle Detection on a Chip. Microfluidic chips are cost-effective and compact and thus well-suited for deployment in resource-limited settings for

DOI: 10.1021/acs.analchem.5b01381
Anal. Chem. 2015, 87, 6434–6445

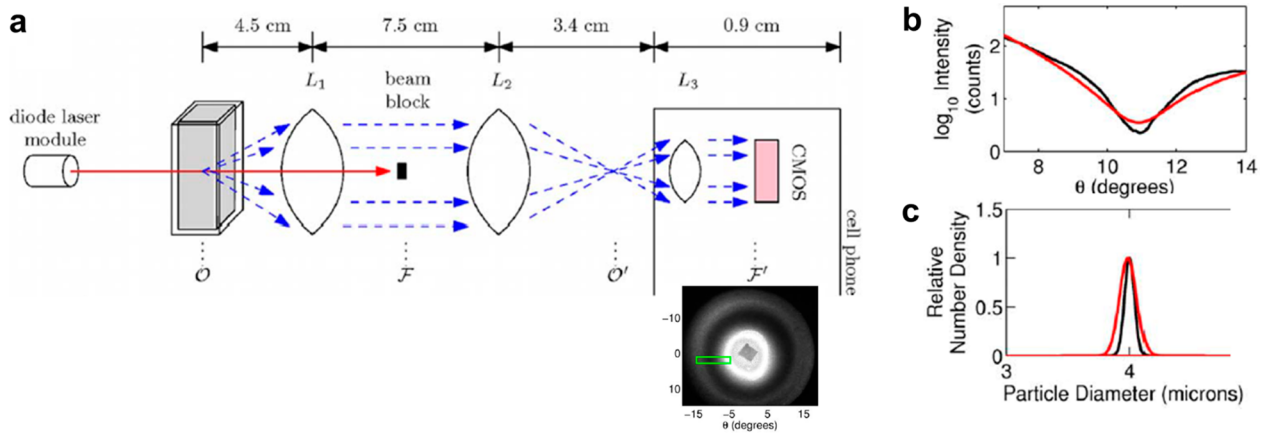

Figure 3. Light scattering based nanocharacterization tools. (a–c) Sizing particles with nanometer accuracy by scattering measurements using a mobile phone camera integrated into a benchtop system. (a) Schematic illustration of the optical setup and a representative angular scattering pattern recorded on the cell phone. (b) Measured (black) and Mie theory fitted (red) angle-dependent scattering intensities. (c) Expected (black) and predicted (red) particle size distributions as determined from scattering data. Panels (a–c) are reprinted under the terms of the Creative Commons Attribution License from Smith, Z. J.; Chu, K.; Wachsmann-Hogiu, S. *PLoS One* **2012**, *7*, e46030 (ref 66).

sensing, diagnostics, and measurement applications. Microfluidic devices are frequently employed for detection,[56] sizing,[57] and separation[56] of nanoscale objects in conjugation with optical methods. Using a fluorescence-based labeling strategy, microfluidic platforms have been demonstrated to trap single viruses such as vaccinia virus particles dielectrophoretically and visualize the capture process by staining the viral surface lipid membrane and nucleic acids with lipophilic carbocyanine dyes (e.g., DiOC63) and DNA staining dyes (e.g., Hoechst 33342), respectively.[58] A dual-mode electrical and optical nanoparticle sensing platform has also been developed for multiparameter analysis of single nanoscale objects (Figure 2a–c).[59] This method is based on an optofluidic chip integrated with a nanopore that allows the translocation of individual nanoparticles into the imaging zone (Figure 2a). This device measures both the transient current decrease when a single nanoparticle crosses the nanopore and a fluorescence spike subsequently.[59] These two parameters together with the time lag (Δt) between the two signals provide a multidimensional feature index for each type of nanoparticle (Figure 2b). Using this device, a nanobead mixture (100 and 200 nm) or a fluorescently labeled influenza A H1N1 virus and nanobead (100 nm) mixture have been successfully classified (Figure 2c).[59]

Microfluidic platforms have also been converted into chip-size spectrometers for spectroscopic analysis of nanoscale objects. These microfluidic devices were integrated with dispersive optical elements such as linear variable filters (LVFs)[60] and discrete bandpass filters[61] along the channel. When the nano-objects traversed along the microfluidic channel, the spectral information on the nano-objects was dispersed into spatial signals (Figure 2d). Continuous spectra were obtained in the case of LVF[60] (Figure 2e), while multispectral intensities were recorded by using a discrete set of bandpass filters.[61] The latter has been demonstrated to classify different fluorescent nano-objects and molecules based on the ratiometric intensities at different spectral bands. For example, using only three bandpass filters, the on-chip spectroscopic device can accurately differentiate as many as 11 commonly used fluorophores including fluorescent quantum dot 545 (QD545) and QD565.[61]

DEMOCRATIZATION OF LABEL-FREE NANOSCALE MEASUREMENT TOOLS

Label-free imaging and sensing tools are important for making universal measurements of unknown samples, of previously purified samples, or of nonbiological samples where specific labels do not exist. Whereas label-based sensing often relies on fluorescence emission, label-free nanoscale measurements typically involve measurements of scattered light or of small modulations of the transmitted or reflected light. Label-free measurements can be particularly challenging because nanoscale particles tend to scatter light very weakly, proportional to the sixth power of the particle size, according to the Rayleigh scattering intensity,[62]

$$I_{\text{intens}} = |S|^2 \propto I_0 \lambda^{-4} d^6 \left(\frac{m^2 - 1}{m^2 + 2} \right)^2 \quad (1)$$

where S is the complex amplitude of the scattered electric field, I_0 is the incident intensity, λ is the optical wavelength, d is the diameter of the nanoparticle, and $m = n_p/n_0$ is the relative refractive index of the particle compared to the surrounding medium.

Sensors Based on Light Scattering. For particles with sizes at the upper range of the Rayleigh regime and even into the Mie scattering regime (particle sizes comparable to the wavelength),[63] sensors based on light scattering form a viable option for nanoparticle detection, characterization, and sizing. The most prevalent conventional scattering-based particle sizing methods fall into two categories: (1) dynamic light scattering (DLS), which calculates the hydrodynamic radius of the particles from their diffusion coefficient measured by the time-dependent scattering intensity fluctuation of the sample,[24] and (2) nanoparticle tracking analysis (NTA), which quantifies particle size and size distribution by measuring the rate of Brownian motion of single nanoparticles in solution.[25,64,65] Both technologies however require fairly bulky benchtop instruments.

A particle sizing method with nanometer accuracy has recently been demonstrated by making Mie scattering measurements using a mobile phone camera that is integrated into a benchtop system (Figure 3a–c).[66] In this case, the cell phone camera records the angularly dependent scattering patterns of

DOI: 10.1021/acs.analchem.5b01381
Anal. Chem. 2015, 87, 6434–6445

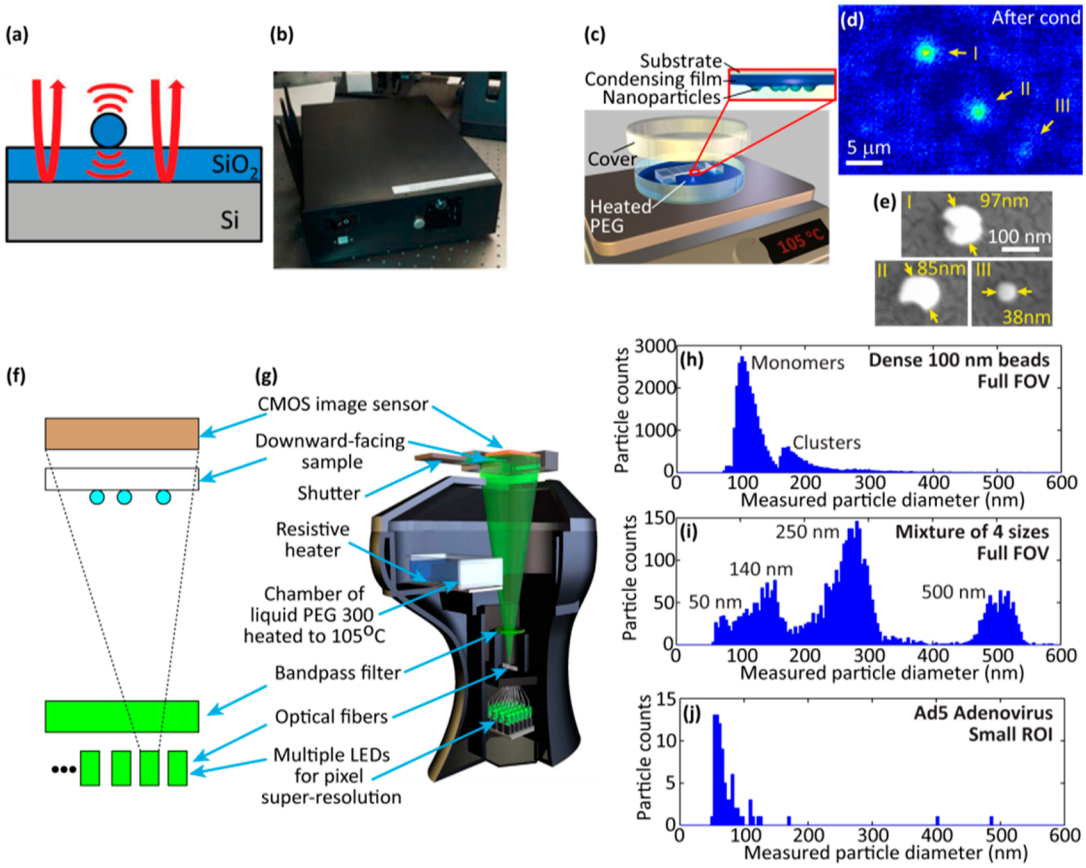

Figure 4. Interferometric imaging and sizing of nanoparticles. (a) Single particle interferometric reflectance imaging sensing (SP-IRIS) scheme. The signal is generated from the interference between the scattered light from the particle and the light reflected from the SiO_2−Si interface. (b) Portable prototype capable of SP-IRIS sensing at the point of care. (c−j) Imaging and sizing of nanoparticles using lensfree holographic on-chip imaging. (c) The condensation of polyethylene glycol (PEG) vapor can be used to form nanolenses that increase the scattering signatures from embedded nanoparticles and enable their detection. (d) Nanoparticles smaller than 40 nm are visible after PEG condensation. (e) Scanning electron microscopy gold-standard comparisons for the particles in (d). (f, g) Line drawing and schematic of a "democratic" nanoscale measurement tool incorporating nanolens formation and imaging. Note that the optical fibers in this design are *multimode* and rather easy to couple light through simple butt coupling. (h−j) Nanoparticle sizing histograms obtained using the device shown in (g). Panel (a) reproduced from Daaboul, G. G.; Yurt, A.; Zhang, X.; Hwang, G. M.; Goldberg, B. B.; Ünlü, M. S. *Nano Lett.* **2010**, *10*, 4727−4731 (ref 70). Copyright 2010 American Chemical Society. Panel (b) is reprinted with permission from Reddington, A. P.; Trueb, J. T.; Freedman, D. S.; Tuysuzoglu, A.; Daaboul, G. G.; Lopez, C. A.; Karl, W. C.; Connor, J. H.; Fawcett, H.; Unlu, M. S. *IEEE Trans. Biomed. Eng.* **2013**, *60*, 3276−3283 (ref 72). Copyright 2013 Institute of Electrical and Electronics Engineers. Panels (c−e) reproduced from McLeod, E.; Nguyen, C.; Huang, P.; Luo, W.; Veli, M.; Ozcan, A. *ACS Nano* **2014**, *8*, 7340−7349 (ref 84). Copyright 2014 American Chemical Society. Panels (g−j) reproduced from McLeod, E.; Dincer, T. U.; Veli, M.; Ertas, Y. N.; Nguyen, C.; Luo, W.; Greenbaum, A.; Feizi, A.; Ozcan, A. *ACS Nano* **2015**, *9*, 3265−3273 (ref 69). Copyright 2015 American Chemical Society.

the particle suspensions by imaging the Fourier plane of the sample onto the cell phone image sensor (Figure 3a). The one-dimensional radial scattering profile was then fitted with Mie theory to estimate the particle size (Figure 3b,c). An average size measurement error of 8 nm was demonstrated for 4, 6, and 8 μm diameter spheres.[66]

Sensors Based on Interferometry. For nanoparticles in the Rayleigh regime (eq 1), the scattered light intensity can be so weak that it is quite challenging to detect it relative to background noise without an additional signal enhancement mechanism. One class of strategies to enhance scattered signal strength is to employ detection mechanisms that have better scaling for small particles, i.e., mechanisms where the scaling exponent on particle size, d, is less than 6. Measuring the interference between the scattered signal and a known reference is one way of reducing the scaling exponent. In such interferometric systems, the directly measured quantity is of the form,

$$I_{\text{interf}} = |R + S|^2 = |R|^2 + SR^* + S^*R + |S|^2 \quad (2)$$

where R and S represent the spatially varying complex fields of the reference wave and scattered wave, respectively. It can often be assumed that the reference wave amplitude and phase are constant and that $|S| \ll |R|$, such that the measured signal is essentially,

$$SR^* + S^*R \approx I_{\text{interf}} - \text{const} \quad (3)$$

Note that here R is a known (i.e., reference) complex constant and that both S and S^* are proportional to $(I_{\text{intens}})^{1/2}$, and therefore, the scaling of the signal on particle size d is reduced from 6 to 3. In practice, the presence of the (S^*R) (twin image or conjugate) term can cause difficulties and potentially corrupt measurements, but its influence can be mitigated through appropriate system design, followed by computation or reconstruction steps.[67−69] The obstacle in implementing interferometric sensing methods in a "democratic" platform often lies in the combination of the reference

DOI: 10.1021/acs.analchem.5b01381
Anal. Chem. 2015, 87, 6434−6445

and scattered beams in a compact, cost-effective, and robust system. This can be challenging for interferometric methods due to their sensitivity to very small changes in optical path lengths, which can result in measurement artifacts due to small vibrations or strains on, e.g., mechanical housings, among other factors.

An interferometric sensing approach that has successfully mitigated these challenges is the single particle interferometric reflectance imaging sensor (SP-IRIS) developed by Selim Ünlü's group at Boston University.[70,71] SP-IRIS sensors are based on common-path interferometry generated by a substrate comprising a ∼100 nm thick silica layer deposited on a silicon wafer. In this geometry, the reference beam is generated due to the reflection at the silica−silicon interface while the scattered signal is generated from a particle sitting at the top of the silica layer (Figure 4a). The small path length difference in this design minimizes the influence of external vibrations or strains on the measured signal. SP-IRIS sensing has been implemented in a simple and easy-to-operate device based on LED illumination and a custom-built microscope using a 0.8 NA microscope objective, which can be used at the point-of-care for viral assays such as Ebola testing (Figure 4b).[72,73] Here, vesicular stomatitis virus particles with sizes of 60−160 nm were specifically captured on the sensor surface (after appropriate surface chemistry steps) and individually detected using SP-IRIS. In addition to virus detection, this approach has also been used to detect aggregates of DNA and protein.[74,75]

Another interferometric approach, developed in our lab, harnesses partially coherent digital in-line holography. We have used lensfree digital holography in cost-effective and robust devices for a range of applications to capture images with a high space-bandwidth product, i.e., images that simultaneously have a very large field of view (>20−30 mm^2) and a high resolution (equivalent to microscope objectives with NA as high as 1.4).[68,76−80] These approaches are highly suited to the democratization of imaging and sensing science because their components can be quite inexpensive. The image sensor chip cost has benefited from the economy of scale for mass production in cell phone cameras, while the light sources rely on standard low-cost LEDs. Furthermore, no expensive microscope objectives are necessary. The rise of the 3D printing industry has also enabled the relatively inexpensive production of device housings even for small quantities that would be requested for use as scientific tools.[81] Despite the high resolution of these lensfree holographic imaging platforms, their ability to detect and measure nanoscale particles can be a challenge, depending on the choice of the optoelectronic sensor chip; for example, the holographic scattering signatures of particles smaller than ∼200−250 nm are typically lost within the background noise of the on-chip imaging system, unless a cooling system is utilized to increase the detection SNR of the imager chip.

To address this challenge and increase the sensitivity of on-chip holographic imaging, we have developed several methods of forming self-assembled on-chip nanolenses that increase the scattering signatures of nanoparticles, enabling their unequivocal detection relative to background noise (Figure 4). These methods include flow-based formation,[82] solvent evaporation,[83] and film-wise condensation of thin polymer films that are stable at room temperatures.[84] Of these approaches, the film-wise condensation of liquid polymers (Figure 4c) has been proven capable of detecting the smallest particles, demonstrating the detection of spherical particles smaller than 40 nm (Figure 4d,e) and rod-shaped particles with diameters smaller than 20 nm using LED illumination with a peak wavelength of ∼510 nm.[84] The enhancement provided by these nanolenses is quantitatively well-understood, as the experimental measurements closely match the predictions of our theory and simulations.[69,84] Furthermore, the signal enhancement and formation of these nanolenses have proved to be highly repeatable, without false positives. All the spots identified using lensfree imaging that are strong enough to indicate particles larger than ∼40−50 nm correspond to real objects on the sample when imaged using SEM. Only when the substrate pretreatment was poorly performed, without being sufficiently hydrophilic, are there any anomalies; however, such cases are easy to identify due to an abnormally extremely dense and contiguous array of spots. Furthermore, as shown in Figure 4f,g, the fabrication and imaging of these nanolenses have been demonstrated in an integrated, field-portable, and cost-effective platform consisting of a resistive heater, a liquid polyethylene glycol chamber, an LED light source, a CMOS image sensor, and a 3D-printed housing.[69] Using this field-portable and "democratic" lensfree imaging platform, tens of thousands of nanoparticles can be sized individually with an accuracy of ±11 nm (Figure 4h−j).

Yet another interferometric approach for the imaging and detection of nanoscale objects is based on a Young interferometer design, where multiple closely spaced parallel coherent beams interfere as they diffract and propagate in free space, reminiscent of Young's famous double-slit experiment.[85,86] In this design, the parallel beams are generated from on-chip waveguides. Light from an external source is first coupled to an on-chip single-mode waveguide. While efficient coupling to single mode waveguides can be time-consuming and dependent on relatively expensive equipment, it is possible to mitigate this challenge through inefficient coupling approaches. As long as the light source provides significantly more power than required by the detector, low-cost focusing lenses and coarse positioning tools can be used to couple light to the waveguides. After coupling, the input waveguide is split into four parallel waveguides using cascaded on-chip splitters, where one of the waveguides is used as a reference wave and the other three are used as sensors, providing the potential for multiplexing. The three parallel measurement waveguides can be functionalized with antibodies for specific analytes such as biomarkers or viruses, whose influence is felt through evanescent coupling with the guided waves. The four waveguides are then cleaved to allow emission into free space. Theoretical performance using multiple wavelengths indicates that concentrations as low as 50 virus particles per milliliter should be detectible.[87] In a compact, field portable device, a similar approach has also been used to detect avian influenza virus with concentrations as low as 5×10^{-4} hemagglutination units per milliliter, where the correspondence between hemagglutination and individual virus particles can vary between 10^4 and 10^7 viruses per hemagglutination unit.[88]

The interference between two beams can also occur entirely within waveguides without the need for free-space propagation. This can further reduce the size of devices providing the potential for extreme miniaturization and field-portability. For especially high sensitivity, optical microcavities can be used as sensing elements. In these approaches, an input waveguide evanescently delivers light to the microcavity, and when the wavelength of this light equals one of the resonances of the microcavity, destructive interference occurs between the light

DOI: 10.1021/acs.analchem.5b01381
Anal. Chem. 2015, 87, 6434−6445

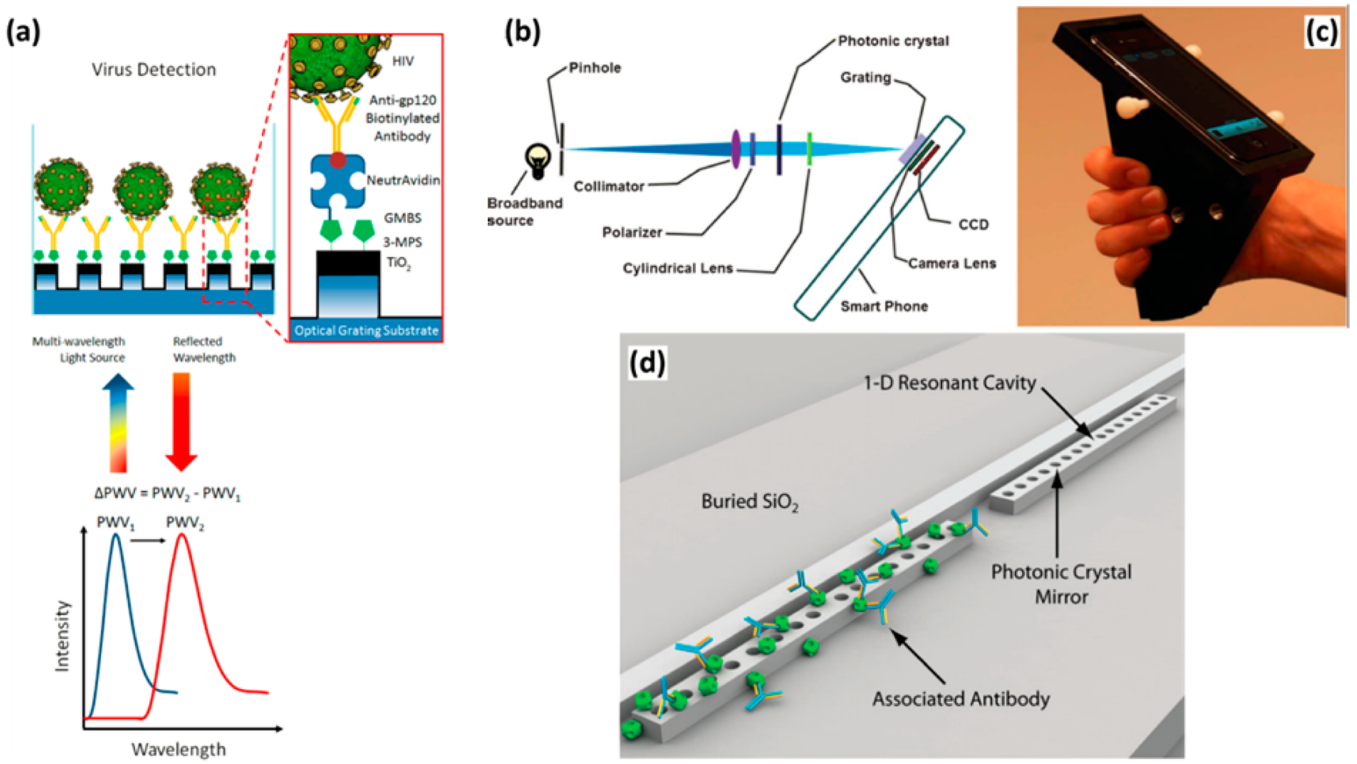

Figure 5. Photonic crystal sensors. (a) Appropriately designed planar photonic crystals generate a narrowband reflection whose peak wavelength shifts upon binding of an analyte such as HIV viral particles. (b, c) Photonic crystal sensing can be implemented in a cost-effective smartphone platform. (c) A photonic crystal oriented in the longitudinal direction parallel to a waveguide can also be used as a narrowband reflector that produces wavelength shift upon binding of an analyte. Panel (a) is reprinted with permission from Shafiee, H.; Lidstone, E. A.; Jahangir, M.; Inci, F.; Hanhauser, E.; Henrich, T. J.; Kuritzkes, D. R.; Cunningham, B. T.; Demirci, U. *Sci. Rep.* **2014**, *4*, 4116 (ref 99). Copyright 2014 Nature Publishing Group. Panels (b) and (c) are reprinted by permission of The Royal Society of Chemistry from Gallegos, D.; Long, K. D.; Yu, H.; Clark, P. P.; Lin, Y.; George, S.; Nath, P.; Cunningham, B. T. *Lab Chip* **2013**, 13, 2124−2132 (ref 97). Copyright 2013 the Royal Society of Chemistry. Panel (d) is reprinted by permission of The Royal Society of Chemistry from Mandal, S.; Goddard, J. M.; Erickson, D. *Lab Chip* **2009**, *9*, 2924−2932 (ref 100). Copyright 2009 the Royal Society of Chemistry.

transmitted through the waveguide and the light leaking from the microcavity back into the waveguide. As an analyte binds to the surface of the microcavity, it alters the local refractive index of the material within the evanescent field of the cavity, which causes the resonant wavelength to shift. These shifts in resonance are tracked by monitoring the relative transmission through the delivery waveguide. High sensitivities are possible because light circulating within the microcavity can interact with each bound analyte molecule millions of times or more.[89] Optical microcavities can include microspheres,[90] microtoroids,[89] glass capillary walls,[91] or microrings,[92] among others. Of these approaches, microrings have thus far found the widest application due to their potential for lithographic mass fabrication and integration with microfluidics due to their planarity. Genalyte has commercialized these sensors; however, they are still at the laboratory scale and not yet at a truly cost-effective or field-portable stage.[93]

Photonic Crystal Sensors. Another resonant sensing approach is based on two-dimensional photonic crystals. These sensors make use of a surface that is structured to have a narrowband (resonant) reflection and/or transmission. At the resonant wavelength, light is coupled from normal incidence into light that propagates transversely along the photonic crystal and is then ultimately reflected and/or transmitted with high efficiency. The most strongly reflected/transmitted wavelength can be altered by the refractive index of the material adsorbed on the surface of the sensor, which interacts evanescently with the light propagating in the photonic crystal. In one transmission-based design, the detection of single particles as small as 150 nm in diameter was observed.[94] While this experiment was performed in a conventional microscope with a 40× microscope objective, monitoring of the photonic crystal could presumably be performed using some of the other field-portable and cost-effective computational imaging approaches presented in this review.

In a reflection-based design,[95] nanoparticles and layers of analyte with nanoscale thickness can be sensed by tracking the modulation of the peak wavelength of the reflected beam (Figure 5a). Conducive to democratization, these photonic crystal-based sensors can be mass-produced out of relatively inexpensive polymer materials using soft-lithography.[96] Furthermore, these devices can be incorporated with a grating-based spectrometer inside a smartphone attachment that correctly aligns the smartphone camera, encapsulating the entire analysis in a field-portable platform (Figure 5b,c).[97] This approach is sensitive enough to detect single 65 nm × 30 nm metal nanoparticles when combined with a microscope system.[98] It has also been used to detect and measure HIV particle concentrations.[99] In an alternative geometry, one-dimensional photonic crystals placed parallel to a waveguide have been used as biosensors that modulate the transmission through the waveguide upon binding of an analyte to the photonic crystal sensor (Figure 5d).[100,101]

DOI: 10.1021/acs.analchem.5b01381
Anal. Chem. 2015, 87, 6434−6445

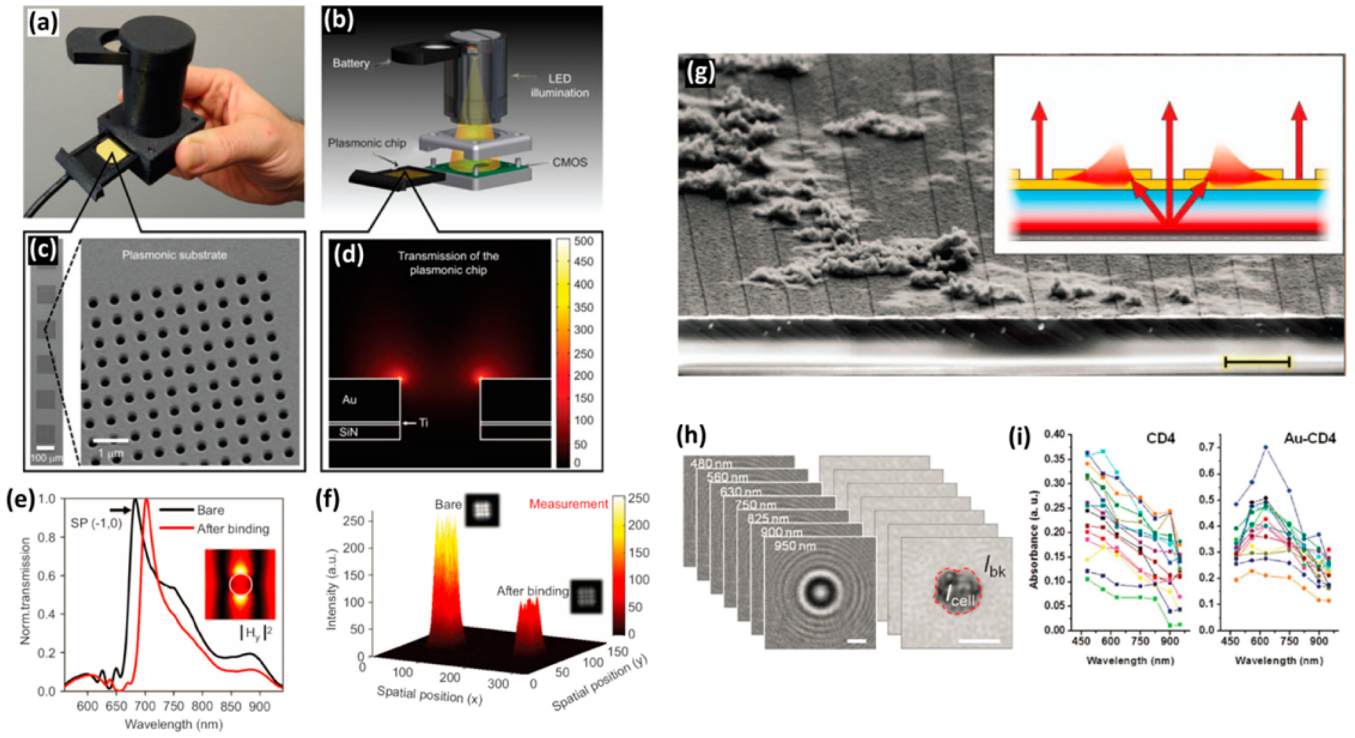

Figure 6. Plasmonic nanosensors. (a, b) Hand-held nanosensor device that includes a light source, plasmonic nanohole array chip, and image sensor chip. (c) Close-up of a nanohole array. (d) Simulation of electric field hot-spots and transmission through the chip. (e) Transmission spectrum before and after the binding of an analyte. (f) Measured response from a single nanohole array before and after analyte binding. (g) Nanostructured plasmonic grating sensor with an embedded quantum well light source. (h) Lensfree imaging of CD4 cells labeled with gold nanoparticles. This technique works as an imaging cytometer by modulating/altering the diffraction patterns of cells that are specifically labeled with particles. (i) Spectra of CD4 cells before and after labeling with gold nanoparticles. The gold plasmon resonance can be seen as a peak around 600 nm. Panels (a–f) are reprinted with permission from Cetin, A. E.; Coskun, A. F.; Galarreta, B. C.; Huang, M.; Herman, D.; Ozcan, A.; Altug, H. *Light Sci. Appl.* **2014**, *3*, e122 (ref 105). Copyright 2014 Nature Publishing Group. Panel (g) is reprinted with permission from Lepage, D.; Jiménez, A.; Beauvais, J.; Dubowski, J. J. *Light Sci. Appl.* **2013**, *2*, e62 (ref 110). Copyright 2013 Nature Publishing Group. Panels (h) and (i) are reprinted with permission from Wei, Q.; McLeod, E.; Qi, H.; Wan, Z.; Sun, R.; Ozcan, A. *Sci. Rep.* **2013**, *3*, 1699 (ref 113). Copyright 2013 Nature Publishing Group.

Plasmonic Sensors. Plasmonic sensors form another successful class of nanoscale measurement tools. For many years, the gold standard in biosensing has been surface plasmon resonance (SPR); however, it has been traditionally limited to rather expensive and bulky instruments.[28] In plasmonic sensors, there is a plasmonic resonance wavelength where light in free space couples very efficiently into plasmonic waves that travel along a metal–dielectric interface. In a similar way to some of the previously discussed sensing approaches, this resonance condition shifts upon specific binding of an analyte due to modulation of the local effective refractive index with which the plasmonic fields interact. The diversity in plasmonic sensors comes from the 3D geometry and nanostructuring, if any, of the metal–dielectric interface.

A promising nanostructured format for plasmonic sensors is a nanohole array, which consists of a very thin metallic substrate with an array of small apertures.[102−104] These substrates exhibit extraordinary optical transmission in that the light transmitted through the array of holes, under appropriate illumination conditions and array design, is greater than the number of holes times the power of light that would be transmitted through a single isolated hole. This extraordinary transmission occurs at specific resonant wavelengths determined by the coupling between free-space waves and surface plasmons confined to the structured substrate. When binding of an analyte occurs on the substrate or within the holes, the spectral resonances of the plasmon mode and the transmitted light shift. Monitoring the transmission of these nanoaperture arrays provides compatibility with lensfree holographic on-chip microscopy platforms similar to those discussed above, and field-portable and cost-effective plasmonic reader devices have already been demonstrated (Figure 6a–f).[105] In the work reported in ref 105, the analyte was not discrete nanoparticles but instead layers of proteins with an effective thickness as small as 3 nm. In another assay, the measurement of the refractive index of bulk liquids, the minimum detectible refractive index change was of the order 10^{-3} refractive index units (RIU).[104−106] The detection is performed by monitoring the loss in transmission of an LED initially tuned to the peak transmission wavelength of the nanohole array. To improve the sensitivity by approximately a factor of 2, ratiometric measurements of two color channels with wavelengths located on either side of the initial resonance can be used in parallel to interrogate the nanohole arrays.[106] Earlier, virus detection experiments had also been shown on a similar plasmonic platform at concentrations in the range of 10^6–10^9 plaque forming units (PFU) per mL.[107] In addition to the imaging/sensing device being cost-effective,[68] the plasmonic substrate/chip can also be cost-effectively fabricated in parallel using high-throughput UV lithography.[106]

We should also note that plasmonic sensors need not be structured in a regular array or uniform fashion. Nonperiodically structured arrays can be used to provide multicolor information in multiplexed assays[108] and to increase spatial

DOI: 10.1021/acs.analchem.5b01381
Anal. Chem. 2015, 87, 6434–6445

resolution or to perform pixel super-resolution.[109] These irregular structures produce diffraction patterns that are specific to both the location of the object (e.g., a fluorescent emitter) and the illumination wavelength. Through a one-time calibration procedure where a narrow beam is scanned across the nanostructured substrate, the correspondence between diffraction patterns and object location (lateral) and wavelength can be determined. Then, when an unknown sample is placed on the same substrate, individual particles or emitters can be computationally imaged/reconstructed and localized with subpixel level resolution on a chip through, e.g., a compressive-sampling approach, even though the raw diffraction patterns of point-emitters are quite large and overlap significantly.[109]

It is also possible to embed light sources within a plasmonic sensing chip for further miniaturization and democratization potential. Jan Dubowski's lab has done this by fabricating quantum well nanostructures underneath a nanostructured metal layer (Figure 6g).[110−112] The quantum wells are excited either through electroluminescence or photoluminescence, and the emitted light is coupled into surface plasmons on the metal layer. Due to nanostructuring on the surface, these surface plasmons can couple into free-space radiation that can be used to make measurements. Similar to other plasmonic devices described earlier, the spectral characteristic of this free-space radiation is highly dependent on the effective refractive index of the material within the evanescent field of the substrate. The sensitivity of these devices has been shown to be quite high with a limit of detection of 1.5×10^{-6} RIU.[110]

Another way in which plasmonic effects can be harnessed is through optical coupling to individual metallic nanoparticles in solution, which can now be obtained commercially at relatively low cost. In this approach, light is coupled to localized surface plasmon modes instead of the propagating surface plasmon polariton modes that were the underlying phenomenon in the previously discussed plasmonic sensors. Nonetheless, metallic nanoparticles also exhibit optical resonances in absorption and scattering, whose wavelengths depend on the size and material composition of the nanoparticles. When nanoparticles aggregate, the effective size of the nanoparticle becomes larger, shifting the resonance wavelength. Wei et al. have utilized this effect using wide-field lensfree holographic on-chip microscopy to differentiate between CD4+ and CD8+ T-cells on a chip (Figure 6h,i).[113] The relative counts of these subpopulations of white blood cells are important in diagnosing AIDS and determining the efficacy of antiretroviral therapy (ART). By using different nanoparticles functionalized for each cell type, it is possible to distinguish such cells, whereas without labeling, these cells are optically indistinguishable, regardless of the spatial resolution of the optical microscope that is being used. Furthermore, the clustering of nanoparticles bound to specific receptors on the cell membrane shifts the plasmon resonance such that these clusters are readily discernible from dispersed/unbound nanoparticles in the solution, even when those dispersed nanoparticles are at relatively high concentrations in the background. Machine learning was also used in this work[113] to further improve the CD4/CD8 classification accuracy, achieving an average accuracy of ∼95% using Au and Ag nanoparticle labeling of CD4+ and CD8+ cells, respectively. Overall, this on-chip technique is equivalent to imaging cytometry as it modulates and accordingly changes the diffraction patterns of different cells that are specifically labeled with particles.

CONCLUSIONS

Here, we have reviewed some of the recent developments in the democratization of optical nanoscale measurement tools based on fluorescence imaging, light scattering, interferometry, photonic crystals, and plasmonics. These emerging devices and techniques are becoming more cost-effective, portable, and user-friendly, providing new opportunities for researchers and citizen scientists, especially in the developing world, to perform advanced measurements and experiments that can globally help to accelerate the rate of discovery and invention and also improve higher education and training of the next generation of scientists and engineers. As we are just at the cusp of these new technologies, the widespread adoption and distribution of devices have thus far been limited; however, we expect rapid growth in the near future. One of the enabling components of rapid expansion in the distribution and adoption of many of these technologies will be the cost reduction involved in fabrication. Soft lithography approaches such as nanoimprint lithography[114] are particularly attractive as they provide a route to scalable, cost-efficient, and "democratic" mass fabrication of structures with nanoscale precision such as those required to make the sensors based on photonic crystals or nanohole arrays. Furthermore, we expect that, as the technologies surrounding mobile phones, image sensors, and 3D printing continue to mature, there will be further reduction in cost and fabrication complexities of these newly emerging nanoscale measurement tools. As Richard P. Feynman once noted:[115] "*There is plenty of room at the bottom*", especially for democratization of nanoscale imaging and sensing tools.

AUTHOR INFORMATION

Corresponding Author

*E-mail: ozcan@ucla.edu. Phone: 1 (310) 825 0915. Web: http://www.innovate.ee.ucla.edu.

Author Contributions

‖E.M. and Q.W. contributed equally.

Notes

The authors declare the following competing financial interest(s): A.O. is the founder of a company that commercializes computational imaging and sensing technologies licensed from UCLA.

ACKNOWLEDGMENTS

The Ozcan Research Group at UCLA gratefully acknowledges the support of the Presidential Early Career Award for Scientists and Engineers (PECASE), the Army Research Office (ARO; W911NF-13-1-0419 and W911NF-13-1-0197), the ARO Life Sciences Division, the ARO Young Investigator Award, the National Science Foundation (NSF) CAREER Award, the NSF CBET Division Biophotonics Program, the NSF Emerging Frontiers in Research and Innovation (EFRI) Award, the NSF EAGER Award, Office of Naval Research (ONR), the Howard Hughes Medical Institute (HHMI), and the National Institutes of Health (NIH) Director's New Innovator Award DP2OD006427 from the Office of the Director, National Institutes of Health. This work is based upon research performed in a laboratory renovated by the National Science Foundation under Grant No. 0963183, which is an award funded under the American Recovery and Reinvestment Act of 2009 (ARRA).

DOI: 10.1021/acs.analchem.5b01381
Anal. Chem. 2015, 87, 6434−6445

REFERENCES

(1) Ozcan, A. *Lab Chip* **2014**, *14*, 3187−3194.
(2) Coskun, A. F.; Wong, J.; Khodadadi, D.; Nagi, R.; Tey, A.; Ozcan, A. *Lab Chip* **2013**, *13*, 636−640.
(3) Coskun, A. F.; Ozcan, A. *Curr. Opin. Biotechnol.* **2014**, *25*, 8−16.
(4) Korpela, E. J.; Anderson, D. P.; Bankay, R.; Cobb, J.; Howard, A.; Lebofsky, M.; Siemion, A. P. V.; von Korff, J.; Werthimer, D. *Proc. SPIE* **2011**, *8152*, DOI: 10.1117/12.894066.
(5) Cooper, C. B.; Dickinson, J.; Phillips, T.; Bonney, R. *Ecol. Soc.* **2007**, *12*, 11.
(6) Robbins, J. Crowdsourcing for the Birds. *New York Times*, August 19, 2013.
(7) Khatib, F.; DiMaio, F.; Group, F. C.; Group, F. V. C.; Cooper, S.; Kazmierczyk, M.; Gilski, M.; Krzywda, S.; Zabranska, H.; Pichova, I.; Thompson, J.; Popovic, Z.; Jaskolski, M.; Baker, D. *Nat. Struct. Mol. Biol.* **2011**, *18*, 1175−1177.
(8) Beberg, A. L.; Ensign, D. L.; Jayachandran, G.; Khaliq, S.; Pande, V. S. In *Parallel and Distributed Processing Symposium, International*; IEEE Computer Society: Los Alamitos, CA, USA, 2009; Vol. *0*, pp 1−8.
(9) Mavandadi, S.; Dimitrov, S.; Feng, S.; Yu, F.; Sikora, U.; Yaglidere, O.; Padmanabhan, S.; Nielsen, K.; Ozcan, A. *PLoS One* **2012**, *7*, No. e37245.
(10) Mavandadi, S.; Dimitrov, S.; Feng, S.; Yu, F.; Yu, R.; Sikora, U.; Ozcan, A. *Lab Chip* **2012**, *12*, 4102−4106.
(11) Mavandadi, S.; Feng, S.; Yu, F.; Dimitrov, S.; Yu, R.; Ozcan, A. *Games Health J.* **2012**, *1*, 373−376.
(12) Ozcan, A. *Sci. Transl. Med.* **2014**, *6*, 233ed9.
(13) Hanay, M. S.; Kelber, S.; Naik, A. K.; Chi, D.; Hentz, S.; Bullard, E. C.; Colinet, E.; Duraffourg, L.; Roukes, M. L. *Nat. Nanotechnol.* **2012**, *7*, 602−608.
(14) Fraikin, J.-L.; Teesalu, T.; McKenney, C. M.; Ruoslahti, E.; Cleland, A. N. *Nat. Nanotechnol.* **2011**, *6*, 308−313.
(15) Wasisto, H. S.; Merzsch, S.; Waag, A.; Uhde, E.; Salthammer, T.; Peiner, E. *Sens. Actuators, B: Chem.* **2013**, *187*, 118−127.
(16) Garza-Licudine, E.; Deo, D.; Yu, S.; Uz-Zaman, A.; Dunbar, W. B. In *2010 Annual International Conference of the IEEE Engineering in Medicine and Biology Society (EMBC)*, Buenos Aires, Argentina, Aug 31 to Sept 4, 2010; pp 5736−5739.
(17) Cybulski, J. S.; Clements, J.; Prakash, M. *PLoS One* **2014**, *9*, No. e98781.
(18) Erickson, D.; Mandal, S.; Yang, A. H. J.; Cordovez, B. *Microfluid. Nanofluid.* **2007**, *4*, 33−52.
(19) De Groot, P.; Deck, L. *J. Mod. Opt.* **1995**, *42*, 389−401.
(20) Aasi, J.; Abadie, J.; Abbott, B. P.; Abbott, R.; Abbott, T. D.; Abernathy, M. R.; Adams, C.; Adams, T.; Addesso, P.; Adhikari, R. X.; et al. *Nat. Photonics* **2013**, *7*, 613−619.
(21) Betzig, E.; Patterson, G. H.; Sougrat, R.; Lindwasser, O. W.; Olenych, S.; Bonifacino, J. S.; Davidson, M. W.; Lippincott-Schwartz, J.; Hess, H. F. *Science* **2006**, *313*, 1642−1645.
(22) Rust, M. J.; Bates, M.; Zhuang, X. *Nat. Methods* **2006**, *3*, 793−796.
(23) Hell, S. W. *Science* **2007**, *316*, 1153−1158.
(24) Berne, B. J.; Pecora, R. *Dynamic Light Scattering: With Applications to Chemistry, Biology, and Physics*; Courier Dover Publications: Mineola, NY, 2000.
(25) Filipe, V.; Hawe, A.; Jiskoot, W. *Pharm. Res.* **2010**, *27*, 796−810.
(26) Kulkarni, P.; Baron, P. A.; Willeke, K. *Aerosol Measurement: Principles, Techniques, and Applications*; John Wiley & Sons: Hoboken, N.J., 2011.
(27) Iida, K.; Stolzenburg, M. R.; McMurry, P. H. *Aerosol Sci. Technol.* **2009**, *43*, 81−96.
(28) Liedberg, B.; Nylander, C.; Lunström, I. *Sens. Actuators* **1983**, *4*, 299−304.
(29) Fan, X.; White, I. M.; Shopova, S. I.; Zhu, H.; Suter, J. D.; Sun, Y. *Anal. Chim. Acta* **2008**, *620*, 8−26.
(30) Ligler, F. S.; Breimer, M.; Golden, J. P.; Nivens, D. A.; Dodson, J. P.; Green, T. M.; Haders, D. P.; Sadik, O. A. *Anal. Chem.* **2002**, *74*, 713−719.
(31) Tempelman, L. A.; King, K. D.; Anderson, G. P.; Ligler, F. S. *Anal. Biochem.* **1996**, *233*, 50−57.
(32) Vashist, S. K.; Mudanyali, O.; Schneider, E. M.; Zengerle, R.; Ozcan, A. *Anal. Bioanal. Chem.* **2013**, *406*, 3263−3277.
(33) A Complete History of the Camera Phone | Digital Trends; http://www.digitaltrends.com/mobile/camera-phone-history/ (accessed Apr 1, 2015).
(34) Koifman, V. Nokia Lumia 1020 Features 1.1 μm BSI Pixel 41MP Sensor. *Image Sensors World*, July 12, 2013.
(35) The World in 2014: ICT Facts and Figures; http://www.itu.int/en/ITU-D/Statistics/Pages/facts/default.aspx (accessed Mar 27, 2015).
(36) Braeckmans, K.; Buyens, K.; Bouquet, W.; Vervaet, C.; Joye, P.; Vos, F. D.; Plawinski, L.; Doeuvre, L.; Angles-Cano, E.; Sanders, N. N.; Demeester, J.; De Smedt, S. C. *Nano Lett.* **2010**, *10*, 4435−4442.
(37) Lakadamyali, M.; Rust, M. J.; Babcock, H. P.; Zhuang, X. *Proc. Natl. Acad. Sci. U. S. A.* **2003**, *100*, 9280−9285.
(38) Rowe, C. A.; Tender, L. M.; Feldstein, M. J.; Golden, J. P.; Scruggs, S. B.; MacCraith, B. D.; Cras, J. J.; Ligler, F. S. *Anal. Chem.* **1999**, *71*, 3846−3852.
(39) Rowe-Taitt, C. A.; Hazzard, J. W.; Hoffman, K. E.; Cras, J. J.; Golden, J. P.; Ligler, F. S. *Biosens. Bioelectron.* **2000**, *15*, 579−589.
(40) Ligler, F. S. *Anal. Chem.* **2009**, *81*, 519−526.
(41) Ligler, F. S.; Sapsford, K. E.; Golden, J. P.; Shriver-Lake, L. C.; Taitt, C. R.; Dyer, M. A.; Barone, S.; Myatt, C. J. *Anal. Sci.* **2007**, *23*, 5−10.
(42) Breslauer, D. N.; Maamari, R. N.; Switz, N. A.; Lam, W. A.; Fletcher, D. A. *PLoS One* **2009**, *4*, No. e6320.
(43) Zhu, H.; Yaglidere, O.; Su, T.-W.; Tseng, D.; Ozcan, A. *Lab Chip* **2011**, *11*, 315−322.
(44) Zhu, H.; Mavandadi, S.; Coskun, A. F.; Yaglidere, O.; Ozcan, A. *Anal. Chem.* **2011**, *83*, 6641−6647.
(45) Zhu, H.; Sikora, U.; Ozcan, A. *Analyst* **2012**, *137*, 2541−2544.
(46) Coskun, A. F.; Nagi, R.; Sadeghi, K.; Phillips, S.; Ozcan, A. *Lab Chip* **2013**, *13*, 4231−4238.
(47) Rajendran, V. K.; Bakthavathsalam, P.; Ali, B. M. J. *Microchim. Acta* **2014**, *181*, 1815−1821.
(48) Zhu, H.; Sencan, I.; Wong, J.; Dimitrov, S.; Tseng, D.; Nagashima, K.; Ozcan, A. *Lab Chip* **2013**, *13*, 1282−1288.
(49) Wei, Q.; Qi, H.; Luo, W.; Tseng, D.; Ki, S. J.; Wan, Z.; Göröcs, Z.; Bentolila, L. A.; Wu, T.-T.; Sun, R.; Ozcan, A. *ACS Nano* **2013**, *7*, 9147−9155.
(50) Wei, Q.; Luo, W.; Chiang, S.; Kappel, T.; Mejia, C.; Tseng, D.; Chan, R. Y. L.; Yan, E.; Qi, H.; Shabbir, F.; Ozkan, H.; Feng, S.; Ozcan, A. *ACS Nano* **2014**, *8*, 12725−12733.
(51) Kim, J.; Johnson, M.; Hill, P.; Gale, B. K. *Integr. Biol.* **2009**, *1*, 574−586.
(52) Rasmussen, K. H.; Marie, R.; Lange, J. M.; Svendsen, W. E.; Kristensen, A.; Mir, K. U. *Lab Chip* **2011**, *11*, 1431−1433.
(53) Lagally, E. T.; Medintz, I.; Mathies, R. A. *Anal. Chem.* **2001**, *73*, 565−570.
(54) Famulok, M.; Hartig, J. S.; Mayer, G. *Chem. Rev.* **2007**, *107*, 3715−3743.
(55) Polonschii, C.; David, S.; Tombelli, S.; Mascini, M.; Gheorghiu, M. *Talanta* **2010**, *80*, 2157−2164.
(56) Blom, M. T.; Chmela, E.; Oosterbroek, R. E.; Tijssen, R.; van den Berg, A. *Anal. Chem.* **2003**, *75*, 6761−6768.
(57) Kuyper, C. L.; Budzinski, K. L.; Lorenz, R. M.; Chiu, D. T. *J. Am. Chem. Soc.* **2006**, *128*, 730−731.
(58) Akin, D.; Li, H.; Bashir, R. *Nano Lett.* **2004**, *4*, 257−259.
(59) Liu, S.; Zhao, Y.; Parks, J. W.; Deamer, D. W.; Hawkins, A. R.; Schmidt, H. *Nano Lett.* **2014**, *14*, 4816−4820.
(60) Schmidt, O.; Bassler, M.; Kiesel, P.; Knollenberg, C.; Johnson, N. *Lab Chip* **2007**, *7*, 626−629.
(61) Cho, S. H.; Qiao, W.; Tsai, F. S.; Yamashita, K.; Lo, Y.-H. *Appl. Phys. Lett.* **2010**, *97*, 093704.
(62) Rayleigh, L. *Philos. Mag. Ser. 5* **1899**, *47*, 375−384.
(63) Mie, G. *Ann. Phys.* **1908**, *330*, 377−445.

DOI: 10.1021/acs.analchem.5b01381
Anal. Chem. 2015, 87, 6434−6445

(64) Xu, C. S.; Cang, H.; Montiel, D.; Yang, H. *J. Phys. Chem. C* **2007**, *111*, 32−35.
(65) Malloy, A. *Mater. Today* **2011**, *14*, 170−173.
(66) Smith, Z. J.; Chu, K.; Wachsmann-Hogiu, S. *PLoS One* **2012**, *7*, No. e46030.
(67) Gorocs, Z.; Ozcan, A. *Biomed. Eng. IEEE Rev.* **2013**, *6*, 29−46.
(68) Mudanyali, O.; Tseng, D.; Oh, C.; Isikman, S. O.; Sencan, I.; Bishara, W.; Oztoprak, C.; Seo, S.; Khademhosseini, B.; Ozcan, A. *Lab. Chip* **2010**, *10*, 1417−1428.
(69) McLeod, E.; Dincer, T. U.; Veli, M.; Ertas, Y. N.; Nguyen, C.; Luo, W.; Greenbaum, A.; Feizi, A.; Ozcan, A. *ACS Nano* **2015**, *9*, 3265−3273.
(70) Daaboul, G. G.; Yurt, A.; Zhang, X.; Hwang, G. M.; Goldberg, B. B.; Ünlü, M. S. *Nano Lett.* **2010**, *10*, 4727−4731.
(71) Monroe, M. R.; Daaboul, G. G.; Tuysuzoglu, A.; Lopez, C. A.; Little, F. F.; Ünlü, M. S. *Anal. Chem.* **2013**, *85*, 3698−3706.
(72) Reddington, A. P.; Trueb, J. T.; Freedman, D. S.; Tuysuzoglu, A.; Daaboul, G. G.; Lopez, C. A.; Karl, W. C.; Connor, J. H.; Fawcett, H.; Unlu, M. S. *IEEE Trans. Biomed. Eng.* **2013**, *60*, 3276−3283.
(73) Daaboul, G. G.; Lopez, C. A.; Chinnala, J.; Goldberg, B. B.; Connor, J. H.; Ünlü, M. S. *ACS Nano* **2014**, *8*, 6047−6055.
(74) Cheng, X. R.; Daaboul, G. G.; Ünlü, M. S.; Kerman, K. *Analyst* **2014**, *139*, 59−65.
(75) Ozkumur, E.; Ahn, S.; Yalçin, A.; Lopez, C. A.; Cevik, E.; Irani, R. J.; DeLisi, C.; Chiari, M.; Unlü, M. S. *Biosens. Bioelectron.* **2010**, *25*, 1789−1795.
(76) Greenbaum, A.; Luo, W.; Su, T.-W.; Göröcs, Z.; Xue, L.; Isikman, S. O.; Coskun, A. F.; Mudanyali, O.; Ozcan, A. *Nat. Methods* **2012**, *9*, 889−895.
(77) Greenbaum, A.; Luo, W.; Khademhosseinieh, B.; Su, T.-W.; Coskun, A. F.; Ozcan, A. *Sci. Rep.* **2013**, *3*, 1717.
(78) Greenbaum, A.; Akbari, N.; Feizi, A.; Luo, W.; Ozcan, A. *PLoS One* **2013**, *8*, No. e76475.
(79) McLeod, E.; Luo, W.; Mudanyali, O.; Greenbaum, A.; Ozcan, A. *Lab Chip* **2013**, *13*, 2028−2035.
(80) Luo, W.; Greenbaum, A.; Zhang, Y.; Ozcan, A. *Light Sci. Appl.* **2015**, *4*, No. e261.
(81) The road ahead for 3-D printers; http://www.pwc.com/us/en/technology-forecast/2014/3d-printing/features/future-3d-printing.jhtml (accessed Mar 28, 2015).
(82) Mudanyali, O.; McLeod, E.; Luo, W.; Greenbaum, A.; Coskun, A. F.; Hennequin, Y.; Allier, C. P.; Ozcan, A. *Nat. Photonics* **2013**, *7*, 247−254.
(83) Hennequin, Y.; Allier, C. P.; McLeod, E.; Mudanyali, O.; Migliozzi, D.; Ozcan, A.; Dinten, J.-M. *ACS Nano* **2013**, *7*, 7601−7609.
(84) McLeod, E.; Nguyen, C.; Huang, P.; Luo, W.; Veli, M.; Ozcan, A. *ACS Nano* **2014**, *8*, 7340−7349.
(85) Ymeti, A.; Greve, J.; Lambeck, P. V.; Wink, T.; van Hövell, S. W. F. M.; Beumer, T. A. M.; Wijn, R. R.; Heideman, R. G.; Subramaniam, V.; Kanger, J. S. *Nano Lett.* **2007**, *7*, 394−397.
(86) Ymeti, A.; Subramaniam, V.; Beumer, T. A.; Kanger, J. S. *Expert Rev. Med. Devices* **2007**, *4*, 447−454.
(87) Mulder, H. K. P.; Ymeti, A.; Subramaniam, V.; Kanger, J. S. *Opt. Express* **2012**, *20*, 20934−20950.
(88) Xu, J.; Suarez, D.; Gottfried, D. S. *Anal. Bioanal. Chem.* **2007**, *389*, 1193−1199.
(89) Armani, D. K.; Kippenberg, T. J.; Spillane, S. M.; Vahala, K. J. *Nature* **2003**, *421*, 925−928.
(90) Vollmer, F.; Arnold, S.; Keng, D. *Proc. Natl. Acad. Sci. U. S. A.* **2008**, *105*, 20701−20704.
(91) Zhu, H.; White, I. M.; Suter, J. D.; Dale, P. S.; Fan, X. *Opt. Express* **2007**, *15*, 9139−9146.
(92) Washburn, A. L.; Luchansky, M. S.; Bowman, A. L.; Bailey, R. C. *Anal. Chem.* **2010**, *82*, 69−72.
(93) Genalyte - Next Generation Multiplexing-Maverick Detection System 858-956-1200; http://genalyte.com/maverick/ (accessed Apr 1, 2015).
(94) Grepstad, J. O.; Kaspar, P.; Solgaard, O.; Johansen, I.-R.; Sudbø, A. S. *Opt. Express* **2012**, *20*, 7954.
(95) Cunningham, B.; Li, P.; Lin, B.; Pepper, J. *Sens. Actuators, B: Chem.* **2002**, *81*, 316−328.
(96) Choi, C. J.; Cunningham, B. T. *Lab Chip* **2006**, *6*, 1373−1380.
(97) Gallegos, D.; Long, K. D.; Yu, H.; Clark, P. P.; Lin, Y.; George, S.; Nath, P.; Cunningham, B. T. *Lab Chip* **2013**, *13*, 2124−2132.
(98) Zhuo, Y.; Hu, H.; Chen, W.; Lu, M.; Tian, L.; Yu, H.; Long, K. D.; Chow, E.; King, W. P.; Singamaneni, S.; Cunningham, B. T. *Analyst* **2014**, *139*, 1007−1015.
(99) Shafiee, H.; Lidstone, E. A.; Jahangir, M.; Inci, F.; Hanhauser, E.; Henrich, T. J.; Kuritzkes, D. R.; Cunningham, B. T.; Demirci, U. *Sci. Rep.* **2014**, *4*, 4116.
(100) Mandal, S.; Goddard, J. M.; Erickson, D. *Lab Chip* **2009**, *9*, 2924−2932.
(101) Mandal, S.; Erickson, D. *Opt. Express* **2008**, *16*, 1623−1631.
(102) Ebbesen, T. W.; Lezec, H. J.; Ghaemi, H. F.; Thio, T.; Wolff, P. A. *Nature* **1998**, *391*, 667−669.
(103) Rindzevicius, T.; Alaverdyan, Y.; Dahlin, A.; Höök, F.; Sutherland, D. S.; Käll, M. *Nano Lett.* **2005**, *5*, 2335−2339.
(104) Khademhosseinieh, B.; Biener, G.; Sencan, I.; Su, T.-W.; Coskun, A. F.; Ozcan, A. *Appl. Phys. Lett.* **2010**, *97*, 221107.
(105) Cetin, A. E.; Coskun, A. F.; Galarreta, B. C.; Huang, M.; Herman, D.; Ozcan, A.; Altug, H. *Light Sci. Appl.* **2014**, *3*, No. e122.
(106) Coskun, A. F.; Cetin, A. E.; Galarreta, B. C.; Alvarez, D. A.; Altug, H.; Ozcan, A. *Sci. Rep.* **2014**, *4*, 6789.
(107) Yanik, A. A.; Huang, M.; Kamohara, O.; Artar, A.; Geisbert, T. W.; Connor, J. H.; Altug, H. *Nano Lett.* **2010**, *10*, 4962−4969.
(108) Khademhosseinieh, B.; Biener, G.; Sencan, I.; Ozcan, A. *Appl. Phys. Lett.* **2010**, *97*, 211112.
(109) Khademhosseinieh, B.; Sencan, I.; Biener, G.; Su, T.-W.; Coskun, A. F.; Tseng, D.; Ozcan, A. *Appl. Phys. Lett.* **2010**, *96*, 171106.
(110) Lepage, D.; Jiménez, A.; Beauvais, J.; Dubowski, J. J. *Light Sci. Appl.* **2013**, *2*, No. e62.
(111) Jimenez, A.; Lepage, D.; Beauvais, J.; Dubowski, J. J. *Microelectron. Eng.* **2012**, *93*, 91−94.
(112) Lepage, D.; Dubowski, J. J. *Biosensors* **2013**, *3*, 201−210.
(113) Wei, Q.; McLeod, E.; Qi, H.; Wan, Z.; Sun, R.; Ozcan, A. *Sci. Rep.* **2013**, *3*, 1699.
(114) Guo, L. J. *Adv. Mater.* **2007**, *19*, 495−513.
(115) Feynman, R. P. *Eng. Sci.* **1960**, *23*, 22−36.

DOI: 10.1021/acs.analchem.5b01381
Anal. Chem. 2015, 87, 6434−6445